

Exploring the Impacts from Datasets to Monocular Depth Estimation (MDE) Models with MineNavi

Wang Xiangtong, Liang Binbin, Yang Menglong, and Li Wei,

Abstract—Current computer vision tasks based on deep learning require a huge amount of data with annotations for model training or testing, especially in some dense estimation tasks, such as optical flow segmentation and depth estimation. In practice, manual labeling for dense estimation tasks is very difficult or even impossible, and the scenes of the dataset are often restricted to a small range, which dramatically limits the development of the community. To overcome this deficiency, we propose a synthetic dataset generation method to obtain the expandable dataset without burdensome manual workforce. By this method, we construct a dataset called MineNavi containing video footages from first-perspective-view of the aircraft matched with accurate ground truth for depth estimation in aircraft navigation application. We also provide quantitative experiments to prove that pre-training via our MineNavi dataset can improve the performance of depth estimation model and speed up the convergence of the model on real scene data. Since the synthetic dataset has a similar effect to the real-world dataset in the training process of deep model, we also provide additional experiments with monocular depth estimation method to demonstrate the impact of various factors in our dataset such as lighting conditions and motion mode.

Index Terms—MineNavi, Synthetic Dataset, Monocular Depth Estimation

1 INTRODUCTION

IN recent years, the machine learning based depth estimation methods, which heavily rely on the labeled dataset, have achieved satisfying performance. However, the scarcity of available labeled data, high costs of data acquisition and annotation, limit the quantity and variety of existing deep learning methods. Although the problem of data shortage can be partly solved by unsupervised learning methods with only sparse or even no annotated data, the ground-truth are still needed in experiments for evaluating or testing the generalization performance of the model. Thus, it is still of great significance to obtain a sufficient amount of images with accurate and dense depth information. The common data acquisition method in real world is not feasible for the depth estimation, especially for aircraft visual navigation because humans cannot manually label a pixel-wise annotation. Building a virtual world to generate synthetic datasets as the intermediate domain with the help of digital simulation technology may be the most feasible way for data generation and labeling at current stage. Since the newly released synthetic datasets[1], [2], [3], [4] are not flexible enough to suit for different needs, e.g, fixed resolution, limited scenes, low data diversity and huge volume, etc, it is difficult to apply them to the dense estimation task in the large scale environment, especially for the depth estimation in aircraft navigation. Therefore, in this paper, we propose a simple and expandable synthetic dataset generation method, and construct a custom

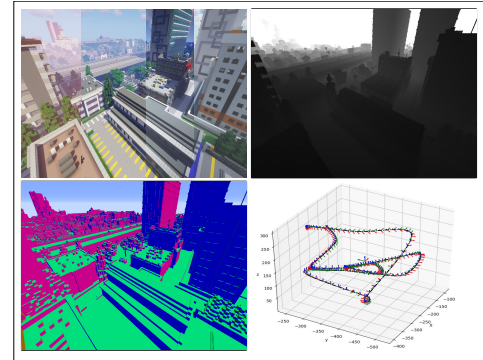


Fig. 1. MineNavi dataset provides image sequence, depth map, surface normal map and camera 6DoF pose in the large scale scene (with over 576m depth).

dataset, which is called as MineNavi (Figure 1). This dataset generation method can not only solve the problem of high cost of real-world data acquisition, but also can narrow the gap between the training domain and the target domain by customizing the synthetic scene that similar with the target domain. Besides, different with conventional studies that adjust models in a fixed dataset to make them close to or superior to the state-of-the-art methods under certain evaluation metrics, we analyze the influences of the changes in datasets on the models. It is very significant because it can not only verify the generalization capabilities of the models to the environment, but also give guidance to construct real-world datasets. In addition, to explore the impact of the various dataset factors on depth estimation models, our constructed MineNavi dataset contains the dense depth

- Li Wei was with the School of Astronautics and Astronautics, Sichuan University, Chengdu, China, 610207.

E-mail: li.wei@scu.edu.cn

Manuscript received xx xx, xxxx; revised xx xx, xxxx.

maps and surface normal vectors of objects. It will help us to observe the performance of depth estimation model under different factors of the dataset, such as the ego-motion camera, lighting and motion patterns, etc. Our experiments show that these variations on training sets may significantly affect the performance of the models.

Our contributions are as follows: firstly, we propose an open synthetic dataset generation method and construct MineNavi for the large-scale depth estimation applications. Secondly, we design experiments to report the performance of the baseline models pre-trained on the MineNavi dataset, and reveal the influence of various factors in datasets on depth estimation models. The source code is available.¹

2 RELATED WORK

2.1 Synthetic Datasets

Using synthetic data has a long history of application in computer vision community [5], [6], [7], [8], [9], it also is a significant data augmentation strategy for data driven models. On one hand, synthesis datasets solve the privacy issues involved in the data collection process partially. On the another hand, the low-level dense prediction tasks, such as optical flow or depth estimation[1], [2], manual annotation is not feasible or even impossible, and synthetic datasets may be the only choice. It is a better idea to use existing scenes from an open-source 3D movie to render artificial annotated data for visual task[2], [1]. Using existing game scenes as data source is an ideal alternative[10], [11], [12], [3], which decrease the cost of manual 3D modeling of scene and realize capturing the data in arbitrary perspectives. Building datasets through open source games can openly and freely allow users to perform differentiated processing for specific vision task and generate the datasets they need, and through rich plug-ins, the cost and difficulty of building data sets can be further reduced to a certain extent.

2.2 Bridging the Reality Gap

Models trained purely on synthetic data often suffer limited generalization caused by domain gap between two type of datasets. Therefore, the utilization and theoretical analysis of the synthetic data set are also very necessary[7]. Domain Randomization (DR)[13] is one of the most promising approaches to make straight-forward transfer learning from synthetic data to real world data. [14] introduced structured domain randomization(SDR) to detection task, which imposes structure onto domain randomization (DR) in order to provide context, they have also shown that pre-training on SDR improves results from real data. [15] represents the composition of a 3D scene with a scene graph and a probabilistic scene grammar, a common representation in computer graphics. Present works[16] have also devoted significant study to domain adaptation(DA), e.g., the problem of adapting models trained on source domain to a previously unseen target domain. In our proposed MineNavi dataset, we implement DR through multiple lighting conditions rendering, switch shader in the same scene and scene replacement of the same path etc. Due to there is a

little overlap between ImageNet and the dataset applied in large-scale depth estimation, MineNavi dataset can be ruled as a intermediate domain for multi-step domain adaptation.

2.3 Datasets Strategy on MDE Training

Although there is a domain gap between synthetic data and real data, most work is based on an assumption that the model trained on real data will perform some results that can be reproduced by training on synthetic data, which leads to the use of synthetic data as a proxy to explore the influence of factors in real data on the model. [6] analyzed the multi-target detection task on different data with different illumination caused by weather conditions. [17] analyzed the influence of background texture and lighting conditions on the task of detecting key points of the object, and concludes that more realistic lighting conditions are beneficial to the performance of the neural network in the task. [18] detailed analysis of the virtual dataset in the optical flow estimation task not only on the impact of lighting, but also included the shape movement and texture of the object. While analysis on above datasets are fairly sufficient, what limits their performance is the lack of the diversity among the benchmark datasets. To this end, [19] makes a synthetic dataset based on CMU Visual Localization dataset[20] and conducts extensive experimental evaluation on the proposed dataset with several learning-based algorithms. [21] introduced a strategy that leverage the mixed datasets in multiple scene for MDE's training. Collecting Large-scale datasets from the Internet[22] is also a way to increase the data diversity, but it require a huge manual labor for data pre- and post-processing.

In this article, we analyze the depth estimation task of weather and lighting conditions, and focus on the influence of camera self-motion, texture and imaging quality on unsupervised monocular depth estimation. To the best of our knowledge, some factors that controlling data source has not been explored before in this context.

3 MINENAVI: A SYNTHETIC DATASET OF LARGE SCALE SCENES

Using MineCraft to construct a dataset is not a novel idea for computer vision community[12], we here to utilize it for depth estimation in aircraft visual navigation application. Our data generation method contains four steps: map loading, camera moving path setting, shader and lighting conditions setting, and ground-truth acquisition. Fig.2 shows the pipeline of data generation process.

Not only the environment features, such as the scene structure and lighting condition, affect the performance of depth estimation models, but also the particular dynamical parameters, such as moving targets in the environment and ego-motion of the aircraft, play important roles in benchmark datasets for models' training and evaluation. Accordingly, each image frame of the dataset can be parameterized as:

$$I[M, P^*(n), s, L(t, w)] \quad (1)$$

where $P^*(n)$ represents the 6 Dof camera motion paths, n is the quantified timestamp of the path, M is the map of the

1. <https://github.com/xdr940/MineNavi>

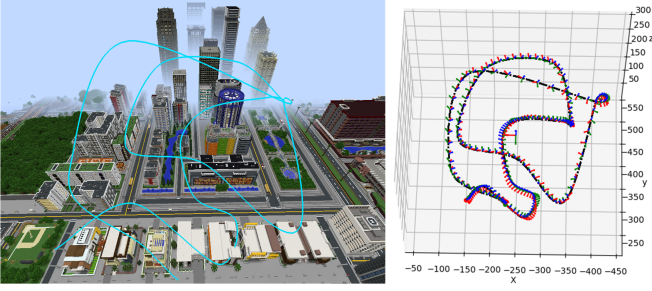


Fig. 4. The accurate camera 6Dof pose at any timestamp in the path is gotten by exporting the key points of the *Aperture* path and interpolating.

In MineNavi, we can set the key points manually or automatically by using *Aperture*² and obtain the full path that matched with image sequence through the interpolation algorithm (See Fig.4). The generated path has high enough dynamics, and the pose transformation is much larger than the general real-world data captured by UAVs.

3.3 Moving Objects in the Scene

The dynamic objects in a practical environment may have a great influence on unsupervised monocular depth estimation method. Many previous work[27], [28], [29] focused on how to remove the negative effects of dynamic objects in monocular depth estimation, but due to the very limited dataset, the progress is far from satisfactory. In order to simulate the influence of a moving object in the synthetic dataset on the depth estimation, the construction of the scene containing moving objects can be further parameterized as:

$$M [P^1(n), P^2(n), \dots, P^m(n)] \quad (6)$$

where P^i is the path of the i th moving objects in the scene. Each of the dynamic object can be modeled as custom shape by *Blender* or other 3d software and set their paths by using *BlockBuster*³. Note that we have no involved the moving object in our proposed dataset yet due to its negative effects on depth estimation model, more details are given in the supplementary material.

3.4 Generating ground-truth annotations

The shader can perform color mapping on the 3D information of the scene, which acts as a ground-truth as shown in Fig.1. We use the *DepthMap* rendering plug-in to export the corresponding error-free, pixel-level dense depth map that matches the image in sequences. In addition, we provide a surface normal rendering plug-in *SurfMap* to support surface normal estimation tasks.

Thus, the datasets construction method proposed in this study can generate a large number of customized datasets at a very low cost. Related code and details are shown in supplementary material.

2. <https://www.curseforge.com/minecraft/mc-mods/aperture>

3. <https://www.curseforge.com/minecraft/mc-mods/blockbuster>

4 PRELIMINARY

In this section, we mainly talk about the principle of MDE models, a analysis method of ego-motion video for MDEs and the relevant dataset for the training and evaluation of MDEs in our experiments.

4.1 Deep Models for Monocular Depth Estimation

In order to reconstruct 3D geometry from the ego-motion video by self-supervised method, the main supervision signal comes from the view synthesis between consecutive frames. We aim to infer the intermediate variable, e.g. predicted depth as precisely as possible through this approach. This is an ill-posed problem because a single 2D image may be produced from a large number of distinct 3D scenes, thus it can only be resolved using prior knowledge about the appearance and motion of image sequences.

Assume that I_t and I_s ($I_s \in \{I_{t-1}, I_{t+1}\}$) are two consecutive frames from an unlabeled video, we want to establish the dense pixel correspondence between the two frames. Let p_t denotes the 2D homogeneous coordinate of a pixel in frame I_t and K denotes the intrinsic camera matrix. We can compute the corresponding point of p_t in frame I_s using the following equation,

$$p_s = K \hat{T}_{t \rightarrow s} \hat{D}_{p_t} K^{-1} p_t \quad (7)$$

where \hat{D}_t is the predicted depth map, and $T_{t \rightarrow s}$ is the relative camera pose. We can get the synthesized image \hat{I}_s , $I_s = I_t(p_s)$. Thus, the photometric error can be formulated as:

$$\mathcal{L}_p = \sum_{s \in \{t^-, t^+\}} \sum_p \rho(I_s(p), \hat{I}_s(p)) \quad (8)$$

where $\rho(\cdot)$ is a function to measure the difference of pixels value in the two images. We use a combination of *SSIM*[30] and *L1* term as our photometric error function which is formulated as:

$$\rho(I, \hat{I}) = \alpha \frac{1 - SSIM(I, \hat{I})}{2} + (1 - \alpha) \|I - \hat{I}\| \quad (9)$$

It is robust to illumination changes in a real-world scenario and we set $\alpha = 0.85$. In general, the photometric loss $\mathcal{L}_p = \rho(I, \hat{I})$.

However, the supervision signal just based on view synthesis is not informative enough in low-texture or homogeneous regions of the scene due to its ambiguities. Thus, additional regularization is required to learn reasonable depth prediction. A common strategy proposed by [31], [32], and it is formulated as :

$$L_s = \sum_{p_t} \sum_{d \in x, y} \|\nabla_d^2 \hat{D}(p_t)\|_1 e^{-\alpha |\nabla_d I_t(p_t)|} \quad (10)$$

where ∇ is the first derivative along the spatial direction. L_s ensures that the edges in depth map are guided by the images. And overall objective function can be formulated as follows:

$$\mathcal{L}_{final}^l = \mathcal{L}_p^l + \lambda \mathcal{L}_s^l \quad (11)$$

where l stands for multi-scale approach.

Unsupervised depth estimation includes monocular methods[31], [32], [26], [25], [24], [33], [34] usually contain

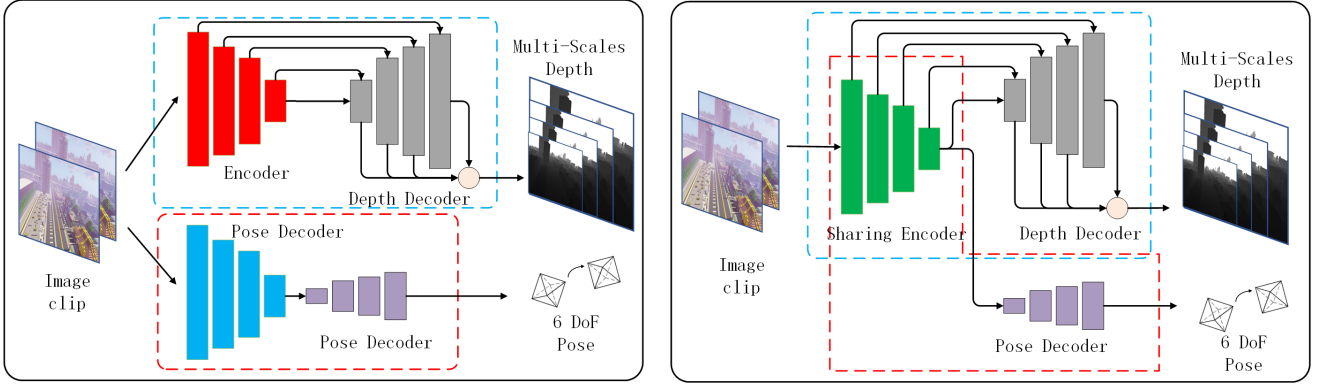


Fig. 5. For spatiotemporal feature learning, We build a 3d encoder and apply it into monodepth2 to build monodepth2-3D (Left) and monodepth2-3Ds (Right)

a single-view depth and a multi-views pose network, to compute the depth. With the similar principle, we use a test model monodepth2[35] and its variants as baseline.

Inspired by spacial-temporal methods in scene understanding[36], [37], the first variant of monodepth2 is monodepth2-3D, i.e., replace the encoder with a 3D encoder for improving the efficiency of training frames, which can enhance the richness by extracting the temporal features from multiple images[28], [38], [39]. What's more, as mentioned by previous work[40] that if there is structural similarity among candidate tasks, it is reasonable to assign just one encoder to extract identical features and recover required information by task-oriented decoders respectively[31], [35]. Thus, we apply the model that using a single encoder to extract the mixed features for depth or pose estimation network as second variants of monodepth2, i.e., monodepth2-3Ds.

4.2 The Sequential Heat-map of Photometric-error Histogram

The unsupervised monocular depth estimation model reconstructs the depth of the scene based on the principle of view synthesis[41], [42], i.e. sfmlerner[31], which offer the main supervisory signal during the training. The quality of the view synthesis seriously affects the performance of the model. Thus, we propose a Sequential Heat-map of Photometric-error Histogram (SHPH) to visualize a image sequence (See Fig.6) and verify weather it is compatible with depth estimation model training intuitively.

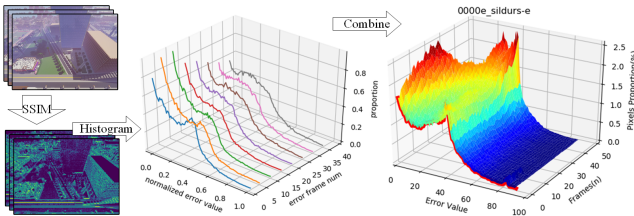


Fig. 6. The process of SHPH. In an image sequence, by normalizing the histogram statistics of any adjacent frame photometric error map, and then connecting together, the heat map that reflect the suitability of training set to MDE could be obtained.

We have found that during the training, the depth estimation models are very sensitive to the distribution of SHPH, The reason behind is that if the photometric error value in the images is evenly distributed, the model can perform more stable during gradient back-propagation, thereby improving the training efficiency. Accordingly, the histogram of each photometric error map in the training sequence should be kept as even as possible, which also provides a basis for choosing a suitable training sequence.

4.3 Datasets

The depth estimation method that based on SfM is not suitable for some datasets due to the absent of successive image[43], [44], large scene scale[45] or applicable camera motion[46], [47], [48]. Therefore in our experiments, we use the follow datasets to make comparison and evaluate the feasibility of the dataset generation method.

- **KITTI** is widely used in monocular depth learning. In this study, we use KITTI Zhou split[31] that contains image triplets, which static frames with an average optical flow of less than 1 pixel are removed. In our experiment 40k triplets are used for training and 4k triplets for testing.
- **FPV**. To test the performance of depth estimation models in the large-sale scenes, we selected the video data of the first person view (FPV) of the aircraft as another experimental dataset. These dataset cover most of the field scenes, including mountains, woods, lakes, snow mountains and cities. Different with previous uav datasets[47], [46] which captured by simple or even static camera motion, this dataset has diverse moving pattern that suitable for depth estimation model based on SfM. We divide the data into two datasets with the train set volume is 36k and 4k validation set.
- **MineNavi** datasets contain data samples according to different shaders(middle-sildurs, high-sildurs), lighting conditions (morning, moon, evening, night, sunny, and rainy), camera motions(linear motion and circular motion) and image qualities (clear, low blur, middle blur, high blur). We set the field of views of camera as 70 degree. The resolutions of the captured

images are 1024×768 . The matched depth map ranges from $0.1m$ to $576m$. Finally, we set more than 400 paths around a virtual scene of more than 16 square kilometers, and collected a total of more than 50,000 image sequences. The image scenes include various weather and lighting conditions, with matching depth values.



Fig. 7. FPV datasets. Left two: Fpv-filed. Right: Fpv-downtown. We introduce FPV dataset to test the generalization of proposed MineNavi dataset.

4.4 Evaluation Metrics

For depth estimation, we evaluate depth estimation models using three accuracy metrics (δ^1 , δ^2 , δ^3) and four error metrics: absolute relative difference (AbsRel), square related difference (SeqRel), RMSE, log RMSE. Note that the accuracy metrics and *AbsRel* are scale-independent, i.e., the value does not change with the depth range of the dataset. And the others are scale-invariants, i.e., the results evaluated on the dataset with different depth ranges are in different order of magnitudes.

5 EXPERIMENTS

In this section, we verify the feasibility and credibility of the MineNavi dataset in the training of the depth estimation model, and explore the impact of dataset varieties on the unsupervised monocular depths estimation model. Thus, we will demonstrate that 1) the depth estimation model can improve generalization through pre-training on MineNavi. 2) it is desirable to exploit the influence of data to model caused by various factors of the dataset. We prepare monodepth2[35] and its two variants monodepth2-3D and monodepth2-3Ds as the test models on our proposed datasets. We also present using Sequential Heat-map of Photometric-error Histogram (SHPH) to verify whether an image sequence is compatible with depth estimation model training intuitively. The detailed description is given in the supplementary material.

5.1 Apply MineNavi to MDE Models

We present two variant models by changing their encoder, and apply them into frameworks of supervised training and unsupervised training (monodepth2). TABLE.1 shows the superiority of multi-frame input models: by simply replacing the encoder from ResNet18 to 3D-ResNet18 and using supervised training method (the model components are identical with monodepth2), they all achieved similar or even better results, and the amount of parameters did not increase, or even reduced by half (monodepth2-3Ds). The quantitative results are shown in Fig.8

It is completely inconsistent with the results of KITTI that multi-frame input models achieve worse results, we suspect that it is because the scenes in KITTI have more moving objects that contradict with Warping-based view synthesis principle, therefore, it may reveal that compared to image input, simple multi-frame input model is superior than single input models in the scenes if the problematic pixels are filtered better.

5.2 Generalization of MineNavi

We execute the models pre-training on MineNavi datasets with linear camera moving path. In order to evaluate the influence of data diversity on the performance, we collect two data samples: the first one contains 10k samples (MN-10K) rendered by high-sildurs shader with the sunny weather, and the second one contains 50K samples (MN-50K) rendered by three shaders (None, middle-sildurs, and high-sildurs) with various lighting conditions (morning, moon, night, and sunny). For comparison, we also prepare the models that are trained from scratch and ImageNet[49]. Although the model pre-trained on ImageNet by classification task has structural difference compare with the model that trained on similar target task, it is still the most popular method in depth estimation task.

5.2.1 Fine-tune on KITTI

We conduct fine-tuning of the monodepth2 and monodepth2-3Ds pre-trained from above datasets on KITTI dataset for 10 epochs.

From TABLE.2 it can be seen that the performance of monodepth2 and monodepth2-3D pre-trained on ImageNet is better than that pre-trained on MN-10k and scratch, but worse than MN-50k. The MineNavi has a strong generalization capability compared to the KITTI. As mentioned before, MN-10k and MN-50k are only different in lighting condition and data volume. Therefore, the diversity of lighting conditions effectively improves the generalization capabilities of the models. Compared with the other datasets, the model of monodepth2-3Ds pre-trained on ImageNet has the better performance. This is mainly because excessive noises in KITTI, e.g, the moving objects deteriorate the robustness of the network performance of the shared encoder, but the large amount of data of ImageNet can make the model more robust[50]. Note that although MineNavi dataset is much smaller the ImageNet, it has competitive performance with ImageNet in depth estimation model training. We also provide qualitative result on Fig.9 and it shows the value in generalization of our MineNavi dataset.

5.2.2 Fine-tune on FPV

Since there is no ground-truth in the FPV dataset, we have to compute the distances between the models in different domains based on the loss value[40]. The closer the migration distance is, the better the pre-training dataset can be generalized to the target domain.

Compared the losses curve among of different pre-trained models that are fine-tuned on FPV in Fig.10, MineNavi pre-trained models converge faster than the others. The reason behind probably comes from that the MineNavi dataset is closer to the FPV dataset than ImageNet in terms

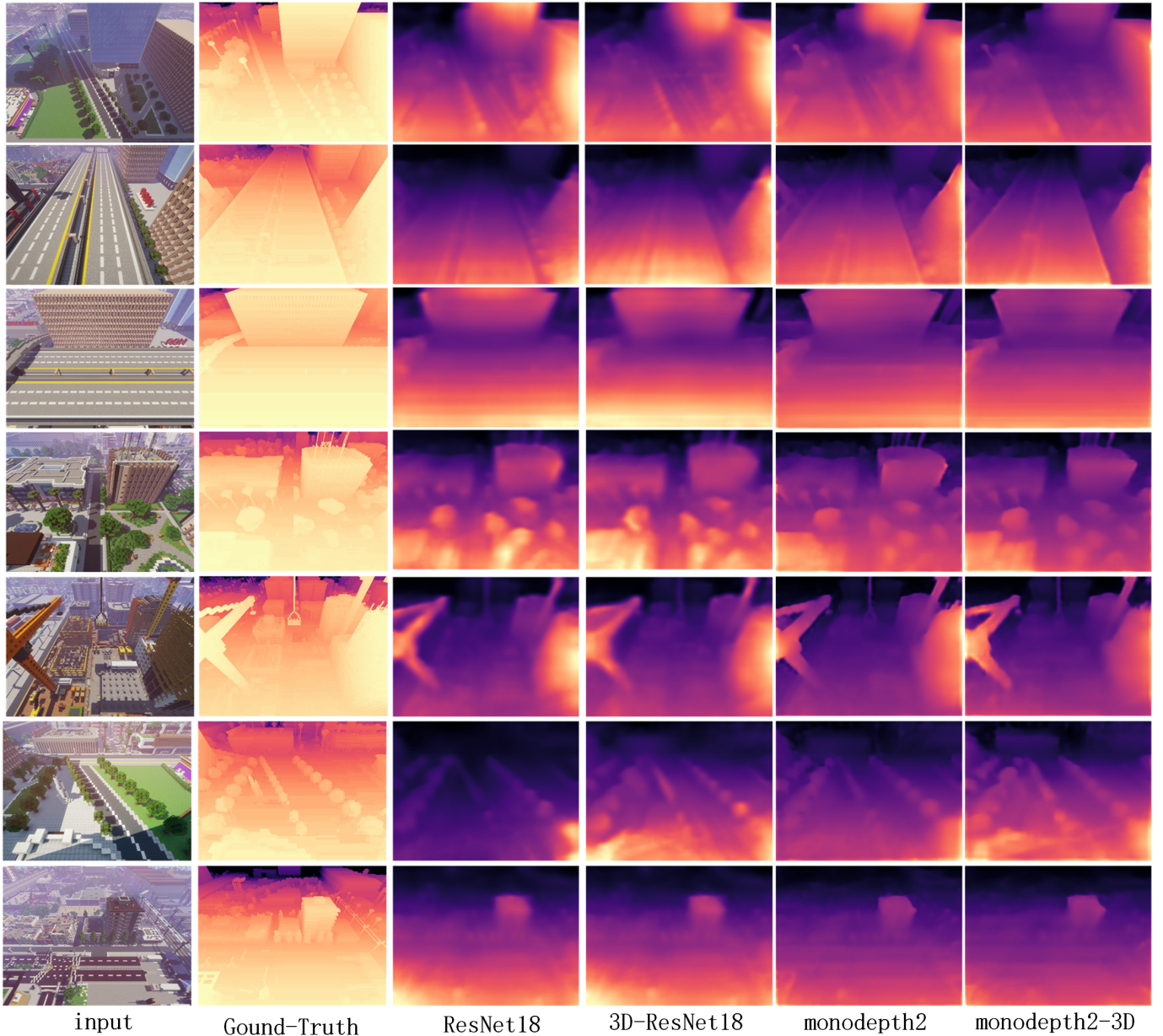


Fig. 8. Qualitative Results of different models in MineNavi.

of environment scenes. What's more, compared with the ImageNet pre-trained model through the task of objects detection, the MineNavi pre-trained model through the task of depth estimation has learned geometric representation[51] during the pre-training, which leads the model converge faster when the target task has structural similarity[40] with source task. Note that, with the continuous expansion of the dataset, MineNavi can realize a more satisfied performance.

5.3 Factors that Affect the Train of MDE

Due to the expandable characteristics of the MineNavi dataset, we can easily generate customized datasets with different variation factors to avoid the over-fitting. It also a helpful way to discover the impacts of factors of datasets on the models. Thus we conduct experiments to explore how the factors in dataset can affect MDE model, including

the shader, lighting conditions, motion blur, ego-motion and velocity of training image sequence.

5.3.1 Impact of Shaders

The MineNavi dataset can generate the rendered image sequences sampled on the same path through different shaders, which allows us to quantitatively evaluate the impacts of the synthetic world design and the quality of other rendering parameters on the algorithm performance. We apply Sildurs⁴ to adjust the image rendering quality and build three datasets *Raw*, *middle-sildurs* and *high-sildurs*. All of them are captured in an identical scene with linear camera motion and collected for 10k samples. The only differences among them are shader setting: *Raw* is rendered by no

4. <https://sildurs-shaders.github.io/>

TABLE 1

Quantitative results in MN datasets. First six model are trained in supervised and the rest are unsupervised (monodepth2).

Model	dataset	Error ↓				Accuracy ↑		
		AbsRel	SqRel	RMS	RMSlog	< 1.25	$< 1.25^2$	$< 1.25^3$
ResNet18	MN-2K(middle)	0.198	1.318	5.679	0.268	0.731	0.923	0.972
3D-ResNet18	MN-2K(middle)	0.194	1.197	5.453	0.259	0.749	0.932	0.973
ResNet18	MN-2K(high)	0.207	1.479	5.832	0.274	0.721	0.920	0.968
3D-ResNet18	MN-2K(high)	0.181	1.159	5.372	0.250	0.761	0.935	0.976
ResNet18	MN-10K(high)	0.142	0.707	4.455	0.181	0.846	0.961	0.986
3D-ResNet18	MN-10K(high)	0.129	0.675	4.384	0.172	0.861	0.966	0.987
monodepth2	MN-2K(high)	0.212	1.426	7.054	0.295	0.706	0.902	0.959
monodepth2-3D	MN-2K(high)	0.245	1.833	5.919	0.273	0.750	0.925	0.965
monodepth2	MN-10K(high)	0.170	0.974	5.782	0.211	0.798	0.941	0.977
monodepth2-3D	MN-10K(high)	0.165	1.170	5.965	0.211	0.800	0.942	0.977
monodepth2-3Ds	MN-10K(high)	0.160	0.991	5.899	0.208	0.809	0.943	0.977

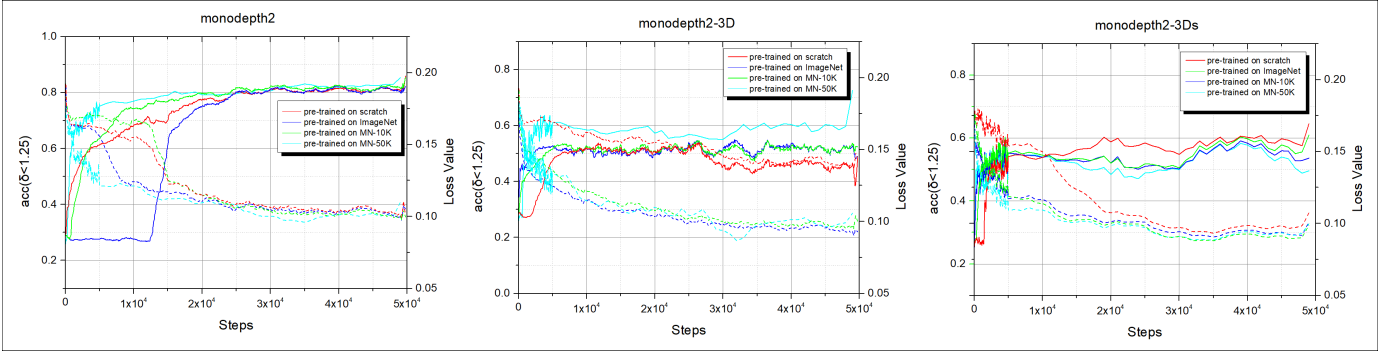
Fig. 9. Fine-tuning curves of three test models on KITTI. Solid curves denote accuracy ($\delta \leq 1.25$) metric of depth estimation and dash curves denote training loss.

TABLE 2

Quantity Results in KITTI with different pre-trained datasets. The best result are bolded and the second best are underlined.

Models	Pre-trained Datasets	Error ↓				Accuracy ↑		
		AbsRel	SqRel	RMS	RMSlog	< 1.25	$< 1.25^2$	$< 1.25^3$
monodepth2	scratch	0.141	1.117	4.797	0.205	0.839	0.948	0.980
	ImageNet	<u>0.135</u>	1.007	<u>4.668</u>	<u>0.200</u>	<u>0.845</u>	<u>0.950</u>	0.980
	MN-10k	0.138	1.095	4.722	0.204	0.843	0.949	0.979
	MN-50k	0.130	<u>1.055</u>	4.630	0.196	0.856	0.953	0.980
monodepth2-3D	scratch	0.170	1.453	5.758	0.247	0.775	0.916	0.963
	ImageNet	0.163	1.857	<u>5.529</u>	0.233	0.807	0.930	0.968
	MN-10k	0.167	2.468	5.671	<u>0.230</u>	<u>0.820</u>	<u>0.932</u>	0.966
	MN-50k	0.153	<u>1.639</u>	5.356	0.224	0.820	0.936	0.970
monodepth2-3Ds	scratch	0.161	1.660	5.449	0.228	0.805	0.930	0.970
	ImageNet	0.158	2.447	<u>5.511</u>	0.220	0.839	0.938	0.970
	MN-10k	0.165	2.361	5.535	0.229	0.820	0.934	0.968
	MN-50k	0.158	<u>2.133</u>	5.555	<u>0.223</u>	<u>0.829</u>	<u>0.936</u>	0.969

shader, *middle-sildurs* uses sildurs with middle performance and *high-sildurs* uses high-performance shader. We apply random initial weights encoder to monodepth2 and train it on above three datasets. We use cross-evaluation on each trained model, i.e., evaluate every model on all datasets. The qualitative results are shown in TABLE.3.

It shows that as the training scenes rendered gradually improve, the performance of the depth estimation model improves consequently. Besides, compared with a model that is trained on less-texture data and tested on rendered data, the model that is trained on rendered data and tested on less-texture data brings a worse result. It is consistent with the fact that the rendering performance will promote the robust of the model during the training.

TABLE 3

The performance of the accuracy of the generated dataset under different rendering shaders. Here *AbsRel* and $\delta < 1.25^1$ are used as error and accuracy indicators. The best result in each row has been underlined and the optimal result has been bolded.

Train Sets (AbsRel \ δ^1)	Test Datasets		
	raw	middle-sildurs	high-sildurs
raw	0.207\0.689	0.326\0.524	0.311\0.528
middle-sildurs	0.436\0.425	0.148\0.813	0.158\0.774
high-sildurs	0.439\0.430	0.156\0.778	0.143\0.816

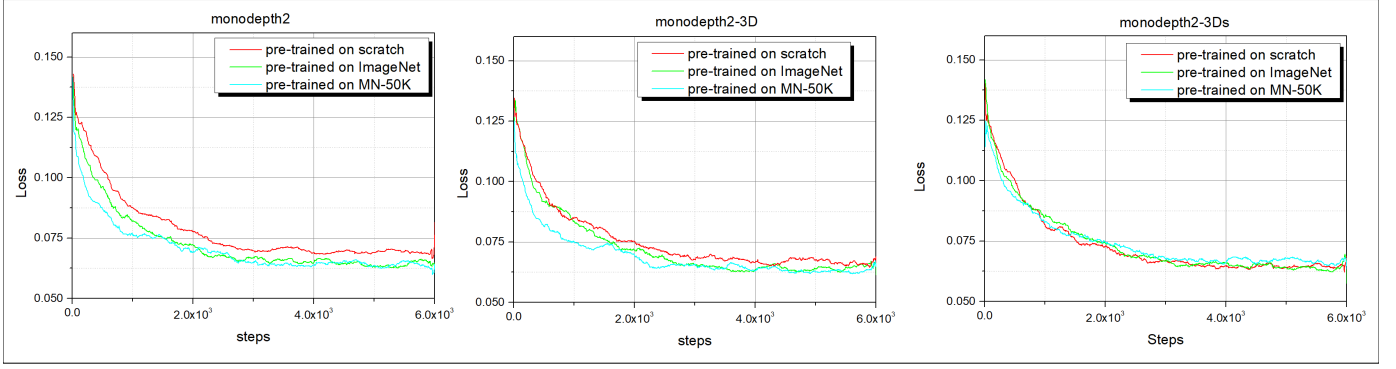


Fig. 10. Fine-tuning curves of three test models on FPV.

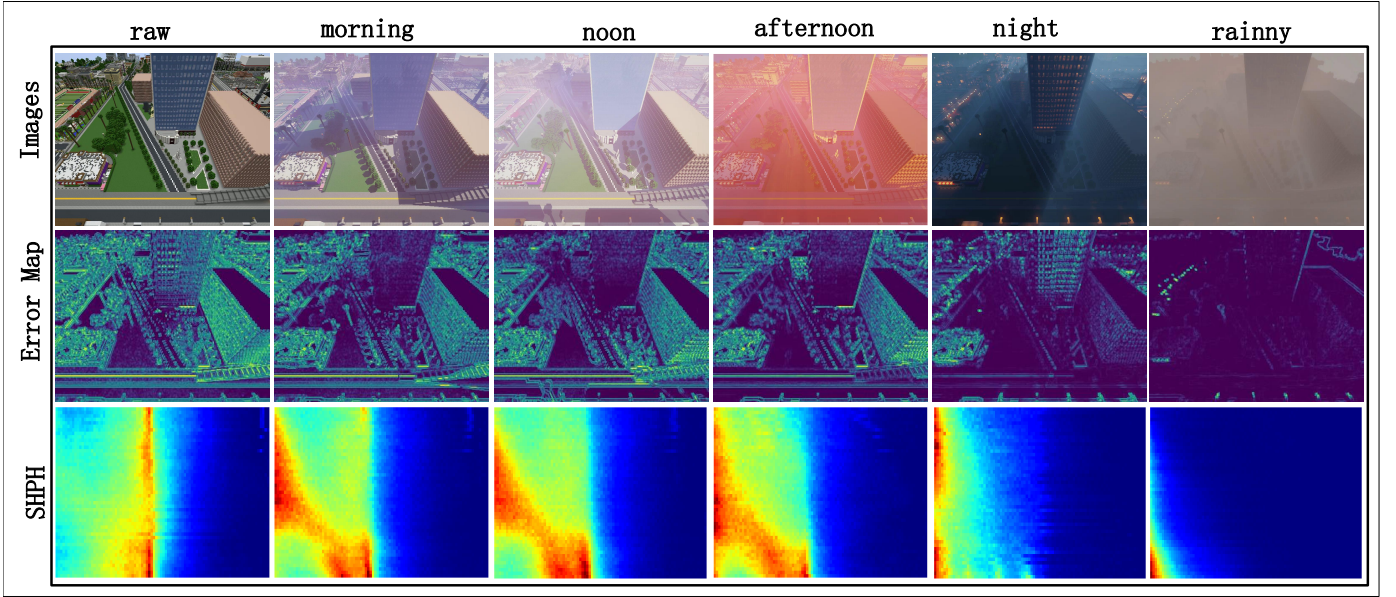
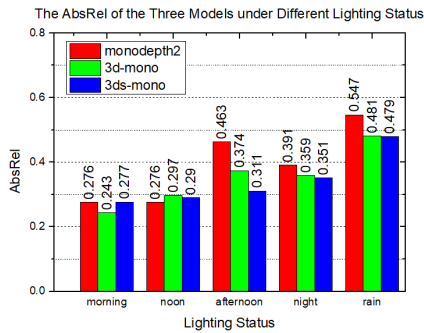


Fig. 11. Sequence under different lighting conditions. Photometric error map (row2) and SHEH map (row3).

Fig. 12. Models trained with datasets that various in lighting conditions show different *AbsRel*.

5.3.2 Lighting Conditions

Previous study[35], [52] show that during the depth estimation model training, the low-texture areas caused by insufficient lighting or overexposure will produce problem pixels in depth estimation.

To further explore the impact of lighting conditions in

data to the depth estimation model, we apply the models with random initial weights and train them on five datasets (See Fig.11) under different lighting conditions: morning, noon, afternoon, night and rainy day. Quantified results on *AbsRel* are shown in Fig.12. We can observe that in the lighting conditions at morning and noon, three test models achieve similar results. However, as the lighting in training data is getting dim (afternoon, night, rainy), three models are deteriorated significantly. This can be attributed primarily to that the adequate lighting makes the color between pixels more diverse, and the error map is close to the uniform distribution. Note that at the time of *afternoon*, the models performance dropped dramatically, even worse than *night* that with dimmer lighting condition, we suspect that the reason behind this is there are too much problematic pixels in captured images caused by lens flare, which strongest in *afternoon* compared with the other lighting conditions. SHPH results on the collected sequences under different lighting conditions and different camera moving paths are shown in the row3 of Fig.11. It can be clearly seen that the clear lighting conditions bring the even distribution of the SHPH.

TABLE 4
Quantity Results in MineNavi with different lights

Models	dataset	Error ↓				Accuracy ↑		
		AbsRel	SqRel	RMS	RMSlog	< 1.25	< 1.25 ²	< 1.25 ³
monodepth2	morning	0.276	8.491	36.672	0.289	0.694	0.885	0.947
	noon	0.276	11.284	49.412	0.321	0.665	0.858	0.931
	afternoon	0.463	26.176	67.480	0.534	0.375	0.647	0.803
	night	0.391	18.674	57.397	0.432	0.470	0.748	0.875
	rain	0.547	30.597	54.880	0.520	0.395	0.671	0.818
monodepth2-3D	morning	0.243	7.469	36.867	0.263	0.737	0.903	0.957
	noon	0.297	11.108	46.373	0.324	0.622	0.852	0.936
	afternoon	0.374	13.967	45.221	0.391	0.478	0.779	0.910
	night	0.359	15.065	49.514	0.392	0.490	0.780	0.907
	rain	0.481	24.776	57.464	0.492	0.386	0.673	0.836
monodepth2-3Ds	morning	0.277	10.086	41.467	0.290	0.697	0.883	0.950
	noon	0.290	11.167	46.460	0.315	0.656	0.865	0.936
	afternoon	0.311	11.901	43.584	0.322	0.618	0.859	0.942
	night	0.351	14.853	52.417	0.384	0.507	0.790	0.906
	rain	0.479	26.123	67.677	0.535	0.349	0.621	0.793

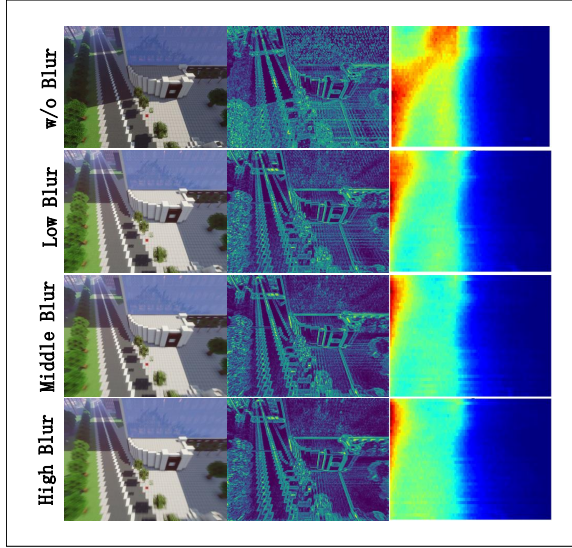


Fig. 13. At close to the ground ($\leq 70m$) a histogram statistical result of the inter-frame error and its sequence photometric error heat map

TABLE 5
The model shows the different accuracy results under different motion blurs

Train Sets (AbsRel \ δ^1)	Test Datasets			
	None	low blur	middle blur	high blur
None	0.221\0.731	0.232\0.705	0.235\0.703	0.237\0.704
low blur	0.237\0.676	0.203\0.731	0.199\0.748	0.201\0.752
middle blur	0.203\0.746	0.177\0.782	0.174\0.811	0.179\0.808
high blur	0.253\0.646	0.213\0.692	0.197\0.729	0.191\0.754

5.3.3 Impact of Motion Blur

The motions of cameras will also affect the stability of the SHPH. As shown in the Fig.13, it can be seen that the distribution of the photometric error map gradually even with the increase motion blur. In our experiment, four datasets with different motion blur are built. The quantified results of monodepth2 are shown in the TABLE.5. The motion blur has a great impact on the SHPH, we suspect that it is

TABLE 6
Motion blur test in monodepth2-3D (up) and monodepth2-3Ds (down).
The best result in each row is underlined and the optimal result is bolded.

Train Sets (AbsRel \ δ^1)	Test Datasets			
	None	low blur	middle blur	high blur
None	0.199\0.768	0.216\0.760	0.217\0.758	0.218\0.752
low blur	0.200\0.730	0.185\0.764	0.184\0.765	0.186\0.764
middle blur	0.194\0.734	0.177\0.775	0.175\0.781	0.176\0.785
high blur	0.200\0.730	0.186\0.763	0.180\0.774	0.181\0.778

Train Sets (AbsRel \ δ^1)	Test Datasets			
	None	low blur	middle blur	high blur
None	0.219\0.739	0.231\0.738	0.235\0.737	0.233\0.735
low blur	0.223\0.704	0.207\0.734	0.206\0.736	0.205\0.737
middle blur	0.228\0.691	0.208\0.726	0.207\0.731	0.207\0.734
high blur	0.246\0.669	0.226\0.704	0.224\0.706	0.223\0.707

an effective way to overcome the noise and introduce the robustness by adding a certain motion blur in sequences. This is reflected in SHPH that appropriate motion blur can make the SHPH more stable, which leads the view synthesis of depth estimation model easier (see Fig.13).

Table 6 shows the the performance of two variants of monodepth2 in MineNavi datasets with different motion blur. It can be seen that the two models are trained on the motion-blurred dataset, and the performance is significantly better than the dataset without blurred.

Besides, we also introduce vary lighting conditions into experiments. As shown in the Table 4, it can be seen that in the variant models of monodepth2, the darker the lighting conditions, the worse the performance, which is consistent with the results of the experiments. Note that at the time of *afternoon*, the models performance dropped dramatically, even worse than *night* that with dimmer lighting condition, We suspect that the reason behind this is there are too much problematic pixels in captured images caused by lens flare, which strongest in *afternoon* compared with the other lighting conditions. It also suggest that the scene fidelity of MineNavi.

TABLE 7
Model performance in different ego-motion modes.

Train\Test Sets (AbsRel \ δ^1)	velocities		
	v_1	v_2	v_3
$\lambda_1 = 1$	0.143\0.816	0.141\0.818	0.152\0.806
$\lambda_2 = \frac{\sqrt{2}}{2}$	0.240\0.472	0.240\0.476	0.252\0.458
$\lambda_3 = 0$	0.280\0.414	0.473\0.234	0.481\0.248

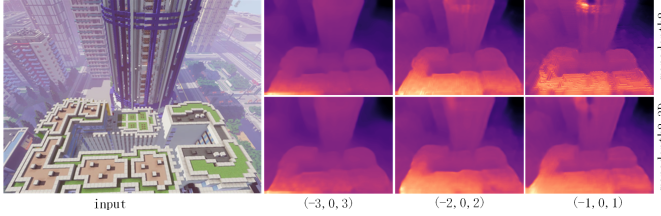


Fig. 14. Qualitative Model Results in MineNavi. First row: monodepth2. Second row: monodepth2-3D. From left to right, the velocity of training sequence is getting lower.

5.3.4 Impact of Ego-motion Variance

The ego-motion of the camera in video will affect the depth estimation model training. Due to the continuous nature of the camera ego-motion, it is not easy to explore the impact of this factor. In this section, we build three datasets that various in motion mode which corresponds to linear motion $\lambda_1 = 1$, overhead cruising motion $\lambda_2 = \frac{\sqrt{2}}{2}$, and circular motion $\lambda_3 = 0$. Finally, the motion speed can be controlled by the number of interval frames of each train triplets in the datasets, and each of them are equipped with three velocity v , and $v_3 > v_2 > v_1$. We test different motion modes through the models, and the quantitative results are shown in the TABLE.7. It can be seen that as the λ decreases, the performance of the test model also decreases, and the velocity of training triplets also has significantly affect on the performance of test model. According to the previous analysis, the reason behind this probably is that the training triplet with larger λ and appropriate velocity have a even distribution in SHPH, hence a better performance is achieved.

5.3.5 Velocity of Training Sequence

We find that the training sequence vary in sample frequency can greatly affect the performance of the model. It is essential because if the velocity of sampling camera is faster, the photometric differences between two adjacent frames are bigger, making the model difficult to train. Fig.14 shows the qualitative results of the models that vary in velocity of training sequence and encoder.

6 CONCLUSION

This paper proposes a method to construct a synthetic dataset, which includes a large-scale scene with low cost but infinite volume, including surface normals, depth, and the 6DoF paths of the camera's ego-motion. This dataset generation method can provide a solution to overcome the difficulty of data collection in some dense estimation

tasks. For depth estimation task in aircraft navigation, we construct several datasets. According to the experimental results, our proposed dataset generation method can perform as an intermediate domain for depth estimation. The data-to-model experiments reveal that future work should not only focus on the innovation of the models, but also pay more attention to the factors in the dataset that affect the models.

REFERENCES

- [1] N. Mayer, E. Ilg, P. Hausser, P. Fischer, D. Cremers, A. Dosovitskiy, and T. Brox, "A large dataset to train convolutional networks for disparity, optical flow, and scene flow estimation," in *Proceedings of the IEEE conference on computer vision and pattern recognition*, 2016, pp. 4040–4048.
- [2] D. J. Butler, J. Wulff, G. B. Stanley, and M. J. Black, "A naturalistic open source movie for optical flow evaluation," in *European Conf. on Computer Vision (ECCV)*, 2012.
- [3] A. Antonini, W. Guerra, V. Murali, T. Sayre-McCord, and S. Karaman, "The blackbird dataset: A large-scale dataset for uav perception in aggressive flight," *CoRR*, 2018.
- [4] Y. Zhang, S. Song, E. Yumer, M. Savva, J.-Y. Lee, H. Jin, and T. Funkhouser, "Physically-based rendering for indoor scene understanding using convolutional neural networks," in *Proceedings of the IEEE Conference on Computer Vision and Pattern Recognition*, 2017, pp. 5287–5295.
- [5] G. Ros, L. Sellart, J. Materzynska, D. Vazquez, and A. M. Lopez, "The synthia dataset: A large collection of synthetic images for semantic segmentation of urban scenes," in *Proceedings of the IEEE conference on computer vision and pattern recognition*, 2016, pp. 3234–3243.
- [6] A. Gaidon, Q. Wang, Y. Cabon, and E. Vig, "Virtualworlds as proxy for multi-object tracking analysis," in *2016 IEEE Conference on Computer Vision and Pattern Recognition (CVPR)*, 2016.
- [7] J. Tremblay, A. Prakash, D. Acuna, M. Brophy, V. Jampani, C. Anil, T. To, E. Cameracci, S. Bochoon, and S. Birchfield, "Training deep networks with synthetic data: Bridging the reality gap by domain randomization," in *Proceedings of the IEEE Conference on Computer Vision and Pattern Recognition Workshops*, 2018, pp. 969–977.
- [8] W. Guerra, E. Tal, V. Murali, G. Ryou, and S. Karaman, "Flight-goggles: Photorealistic sensor simulation for perception-driven robotics using photogrammetry and virtual reality," in *2019 IEEE/RSJ International Conference on Intelligent Robots and Systems (IROS)*. IEEE, 2019, pp. 6941–6948.
- [9] A. Antonini, W. Guerra, V. Murali, T. Sayre-McCord, and S. Karaman, "The blackbird dataset: A large-scale dataset for uav perception in aggressive flight," in *International Symposium on Experimental Robotics*. Springer, 2018, pp. 130–139.
- [10] Q. Wang, J. Gao, W. Lin, and Y. Yuan, "Learning from synthetic data for crowd counting in the wild," in *Proceedings of the IEEE/CVF Conference on Computer Vision and Pattern Recognition*, 2019, pp. 8198–8207.
- [11] S. R. Richter, V. Vineet, S. Roth, and V. Koltun, "Playing for data: Ground truth from computer games," in *European conference on computer vision*. Springer, 2016, pp. 102–118.
- [12] W. H. Guss, B. Houghton, N. Topin, P. Wang, C. Codel, M. Veloso, and R. Salakhutdinov, "Miner1: A large-scale dataset of minecraft demonstrations," in *IJCAI*, 2019.
- [13] J. Tobin, R. Fong, A. Ray, J. Schneider, W. Zaremba, and P. Abbeel, "Domain randomization for transferring deep neural networks from simulation to the real world," in *2017 IEEE/RSJ international conference on intelligent robots and systems (IROS)*. IEEE, 2017, pp. 23–30.
- [14] A. Prakash, S. Bochoon, M. Brophy, D. Acuna, E. Cameracci, G. State, O. Shapira, and S. Birchfield, "Structured domain randomization: Bridging the reality gap by context-aware synthetic data," in *2019 International Conference on Robotics and Automation (ICRA)*. IEEE, 2019, pp. 7249–7255.
- [15] A. Kar, A. Prakash, M.-Y. Liu, E. Cameracci, J. Yuan, M. Rusiniak, D. Acuna, A. Torralba, and S. Fidler, "Meta-sim: Learning to generate synthetic datasets," in *Proceedings of the IEEE/CVF International Conference on Computer Vision*, 2019, pp. 4551–4560.
- [16] M. Wang and W. Deng, "Deep visual domain adaptation: A survey," *Neurocomputing*, vol. 312, pp. 135–153, 2018.

- [17] H. Su, C. R. Qi, Y. Li, and L. J. Guibas, "Render for cnn: View-point estimation in images using cnns trained with rendered 3d model views," in *Proceedings of the IEEE International Conference on Computer Vision*, 2015, pp. 2686–2694.
- [18] N. Mayer, E. Ilg, P. Fischer, C. Hazirbas, D. Cremers, A. Dosovitskiy, and T. Brox, "What makes good synthetic training data for learning disparity and optical flow estimation?" *Int. J. Comput. Vis.*, vol. 126, no. 9, pp. 942–960, 2018.
- [19] H. Hu, B. Yang, Z. Qiao, D. Zhao, and H. Wang, "Seasondepth: Cross-season monocular depth prediction dataset and benchmark under multiple environments," *arXiv preprint arXiv:2011.04408*, 2020.
- [20] H. Badino, D. Huber, and T. Kanade, "Visual topometric localization," in *2011 IEEE Intelligent vehicles symposium (IV)*. IEEE, 2011, pp. 794–799.
- [21] K. Lasinger, R. Ranftl, K. Schindler, and V. Koltun, "Towards robust monocular depth estimation: Mixing datasets for zero-shot cross-dataset transfer," *arXiv preprint arXiv:1907.01341*, 2019.
- [22] Z. Li, T. Dekel, F. Cole, R. Tucker, N. Snavely, C. Liu, and W. T. Freeman, "Learning the depths of moving people by watching frozen people," in *Proceedings of the IEEE/CVF Conference on Computer Vision and Pattern Recognition*, 2019, pp. 4521–4530.
- [23] MineCraftMaps, "minecraftmaps," <https://www.minecraftmaps.com/>, 2011.
- [24] J. Bian, Z. Li, N. Wang, H. Zhan, C. Shen, M.-M. Cheng, and I. Reid, "Unsupervised scale-consistent depth and ego-motion learning from monocular video," *Advances in neural information processing systems*, vol. 32, pp. 35–45, 2019.
- [25] Y. Zou, Z. Luo, and J.-B. Huang, "Df-net: Unsupervised joint learning of depth and flow using cross-task consistency," in *Proceedings of the European conference on computer vision (ECCV)*, 2018, pp. 36–53.
- [26] V. Guizilini, R. Ambrus, S. Pillai, A. Raventos, and A. Gaidon, "3d packing for self-supervised monocular depth estimation," in *IEEE Conference on Computer Vision and Pattern Recognition (CVPR)*, 2020.
- [27] Z. Yin and J. Shi, "Geonet: Unsupervised learning of dense depth, optical flow and camera pose," in *Proceedings of the IEEE conference on computer vision and pattern recognition*, 2018, pp. 1983–1992.
- [28] J. Watson, O. Mac Aodha, V. Prisacariu, G. Brostow, and M. Firman, "The temporal opportunist: Self-supervised multi-frame monocular depth," in *Proceedings of the IEEE/CVF Conference on Computer Vision and Pattern Recognition*, 2021, pp. 1164–1174.
- [29] M. Klingner, J.-A. Termohlen, J. Mikolajczyk, and T. Fingscheidt, "Self-supervised monocular depth estimation: Solving the dynamic object problem by semantic guidance," in *European Conference on Computer Vision*. Springer, 2020, pp. 582–600.
- [30] Z. Wang, A. C. Bovik, H. R. Sheikh, and E. P. Simoncelli, "Image quality assessment: from error visibility to structural similarity," *IEEE transactions on image processing*, vol. 13, no. 4, pp. 600–612, 2004.
- [31] T. Zhou and M. Brown, "Unsupervised learning of depth and ego-motion from video," in *CVPR*, 2017.
- [32] C. Godard and M. Aodha, "Unsupervised monocular depth estimation with left-right consistency," in *CVPR*, 2017.
- [33] A. Ranjan, V. Jampani, L. Balles, K. Kim, D. Sun, J. Wulff, and M. J. Black, "Competitive collaboration: Joint unsupervised learning of depth, camera motion, optical flow and motion segmentation," in *Proceedings of the IEEE/CVF Conference on Computer Vision and Pattern Recognition*, 2019, pp. 12 240–12 249.
- [34] Z. Yang, P. Wang, Y. Wang, W. Xu, and R. Nevatia, "Lego: Learning edge with geometry all at once by watching videos," in *Proceedings of the IEEE conference on computer vision and pattern recognition*, 2018, pp. 225–234.
- [35] C. Godard, O. Mac Aodha, M. Firman, and G. Brostow, "Digging into self-supervised monocular depth estimation," in *CVPR*, 2019.
- [36] N. Li, F. Chang, and C. Liu, "Spatial-temporal cascade autoencoder for video anomaly detection in crowded scenes," *IEEE Transactions on Multimedia*, vol. 23, pp. 203–215, 2020.
- [37] J. Li, X. Liu, W. Zhang, M. Zhang, J. Song, and N. Sebe, "Spatio-temporal attention networks for action recognition and detection," *IEEE Transactions on Multimedia*, vol. 22, no. 11, pp. 2990–3001, 2020.
- [38] J. Hur and S. Roth, "Self-supervised multi-frame monocular scene flow," in *Proceedings of the IEEE/CVF Conference on Computer Vision and Pattern Recognition*, 2021, pp. 2684–2694.
- [39] V. Patil, W. Van Gansbeke, D. Dai, and L. Van Gool, "Don't forget the past: Recurrent depth estimation from monocular video," *IEEE Robotics and Automation Letters*, vol. 5, no. 4, pp. 6813–6820, 2020.
- [40] A. R. Zamir, A. Sax, W. Shen, L. J. Guibas, J. Malik, and S. Savarese, "Taskonomy: Disentangling task transfer learning," in *Proceedings of the IEEE conference on computer vision and pattern recognition*, 2018, pp. 3712–3722.
- [41] R. Garg, V. K. Bg, G. Carneiro, and I. Reid, "Geometry to the rescue," in *European conference on computer vision*. Springer, 2016, pp. 740–756.
- [42] J. Flynn, I. Neulander, J. Philbin, and N. Snavely, "Deepstereo: Learning to predict new views from the world's imagery," in *Proceedings of the IEEE conference on computer vision and pattern recognition*, 2016, pp. 5515–5524.
- [43] Z. Li and N. Snavely, "Megadepth: Learning single-view depth prediction from internet photos," in *Proceedings of the IEEE Conference on Computer Vision and Pattern Recognition*, 2018, pp. 2041–2050.
- [44] P. K. Nathan Silberman, Derek Hoiem and R. Fergus, "Indoor segmentation and support inference from rgb-d images," in *ECCV*, 2012.
- [45] J. Sturm, N. Engelhard, F. Endres, W. Burgard, and D. Cremers, "A benchmark for the evaluation of rgb-d slam systems," in *Proc. of the International Conference on Intelligent Robot Systems (IROS)*, Oct. 2012.
- [46] P. Zhu, L. Wen, X. Bian, H. Ling, and Q. Hu, "Vision meets drones: A challenge," *arXiv preprint arXiv:1804.07437*, 2018.
- [47] M. Barekatin, M. Marti, H.-F. Shih, S. Murray, K. Nakayama, Y. Matsuo, and H. Prendinger, "Okutama-action: An aerial view video dataset for concurrent human action detection," in *Proceedings of the IEEE conference on computer vision and pattern recognition workshops*, 2017, pp. 28–35.
- [48] M. Burri, Nikolic, Gohl, Schneider, Rehder, Omari, W. Achtelek, and Siegwart, "The euroc micro aerial vehicle datasets," *I. J. Robotics Res.*, pp. 1157–1163, 2016.
- [49] D. Jia and W. Dong, "Imagenet: A large-scale hierarchical image database," in *CVPR*, 2009.
- [50] D. Hendrycks, K. Lee, and M. Mazeika, "Using pre-training can improve model robustness and uncertainty," in *International Conference on Machine Learning*. PMLR, 2019, pp. 2712–2721.
- [51] K. Wang, Y. Chen, H. Guo, L. Wen, and S. Shen, "Geometric pretraining for monocular depth estimation," in *2020 IEEE International Conference on Robotics and Automation (ICRA)*. IEEE, 2020, pp. 4782–4788.
- [52] X. Wang, W. Li, M. Yang, P. Cheng, and B. Liang, "Unsupervised monocular training method for depth estimation using statistical masks," *IEEE Access*, vol. 8, pp. 191 530–191 541, 2020.